doi:10.1038/nature23878

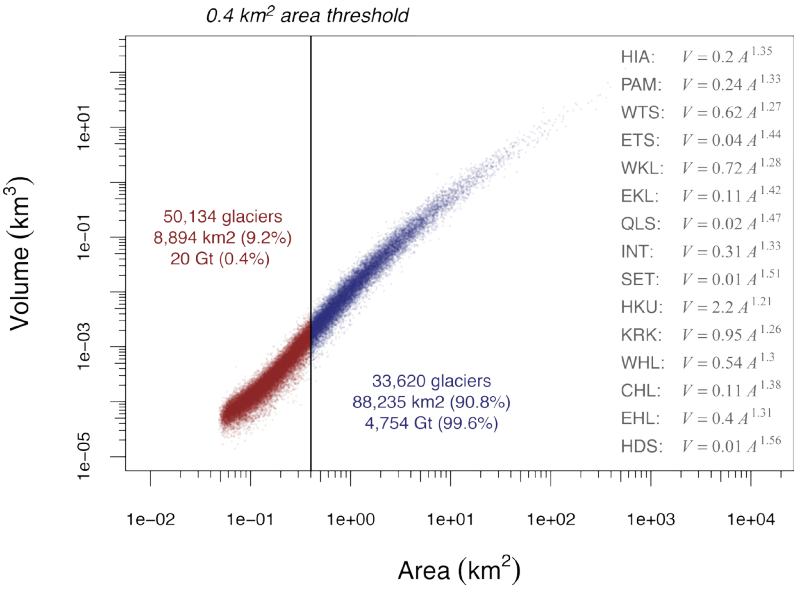

Figure S1 | Relation between area and volume for the entire HMA. The graph shows volume versus area for all glaciers that are larger than 25 Landsat pixels, i.e. 0.0225 km² (n=83,754), based on modelled ice thickness. The glaciers below the 0.4 km² threshold were discarded for further analysis. Volume-area scaling relations for each RGI sub-region were determined using regression and are shown in the plot as grey annotation. Note that these volume-area scaling relationships are shown as additional information for the reader, they were not used in our modelling.

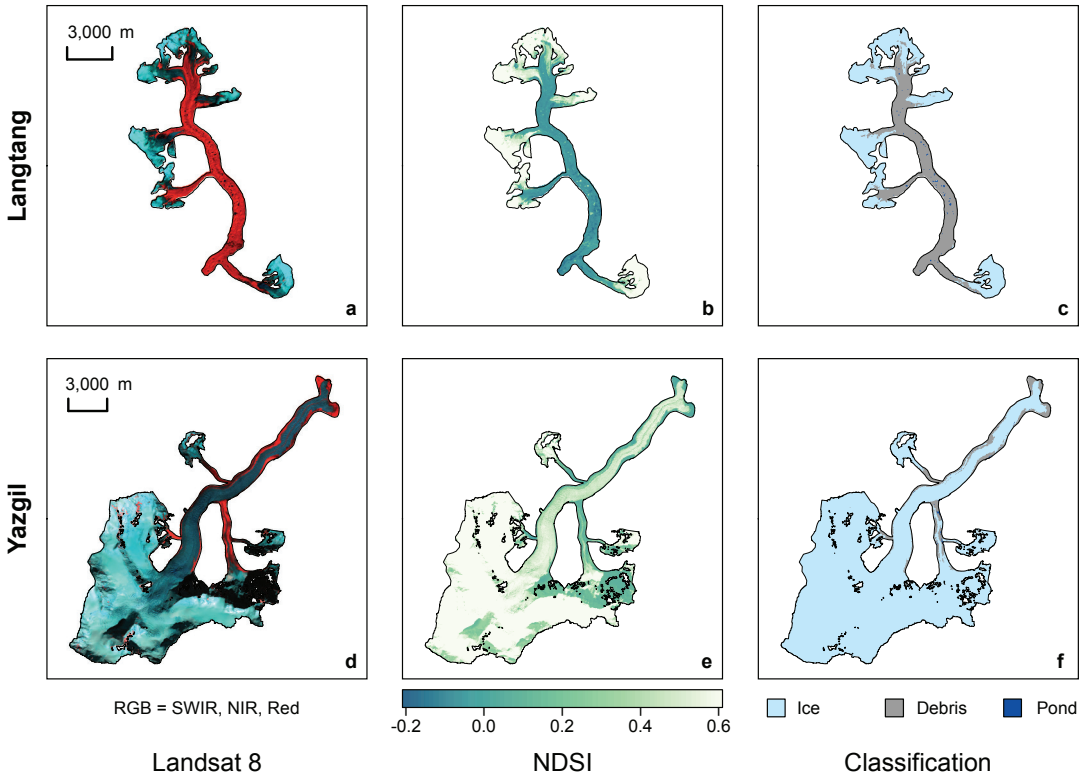

Figure S2 | Example maps of the debris classification. Landsat 8 imagery (**a, d**), Normalised Difference Snow Index (NDSI) (**b, e**) and final debris classification (**c, f**) for the 38 km² Langtang Glacier (**a-c**) and the 134 km² Yazghil Glacier (**d-f**). The RGI glacier outline is depicted as a black line.

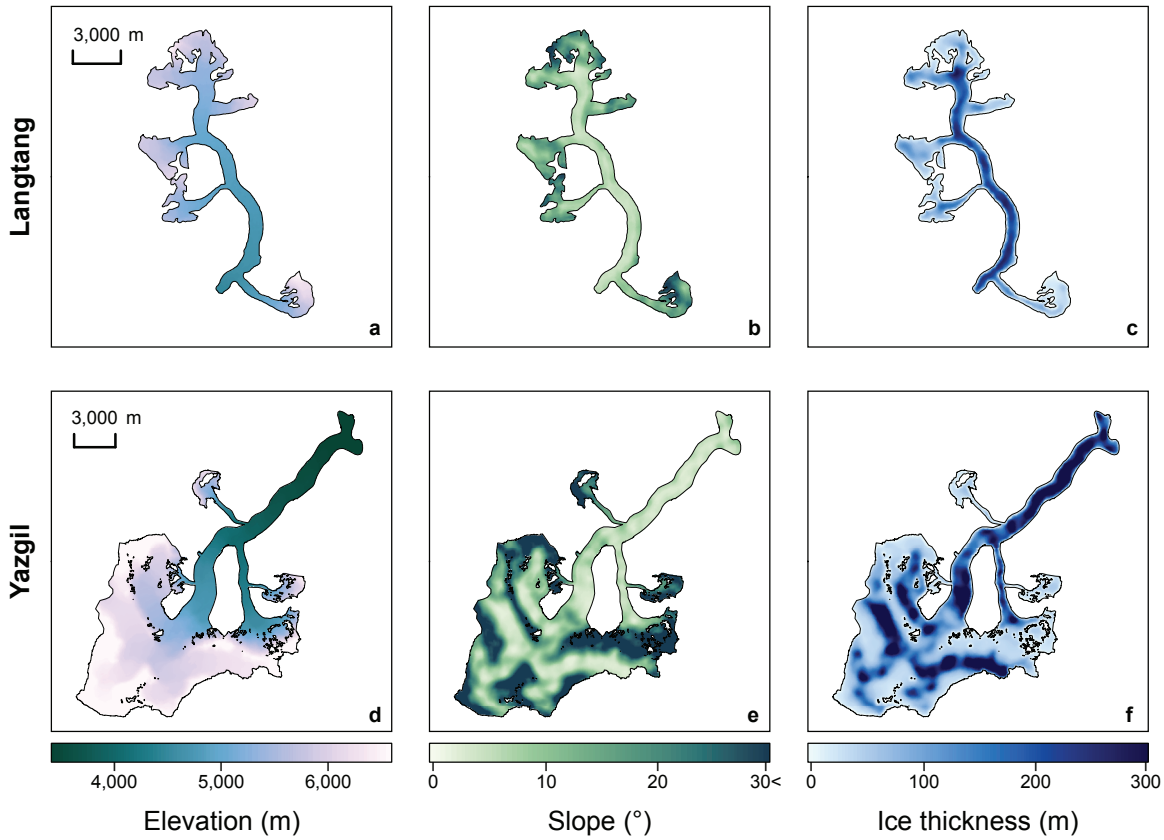

Figure S3 | Example maps of the ice thickness modelling. SRTM elevation (**a, d**), SRTM slope (**b, e**) and GlabTop2 ice thickness (**c, f**) for Langtang Glacier (**a-c**) and Yazghil Glacier (**d-f**). The RGI glacier outline is depicted as a black line.

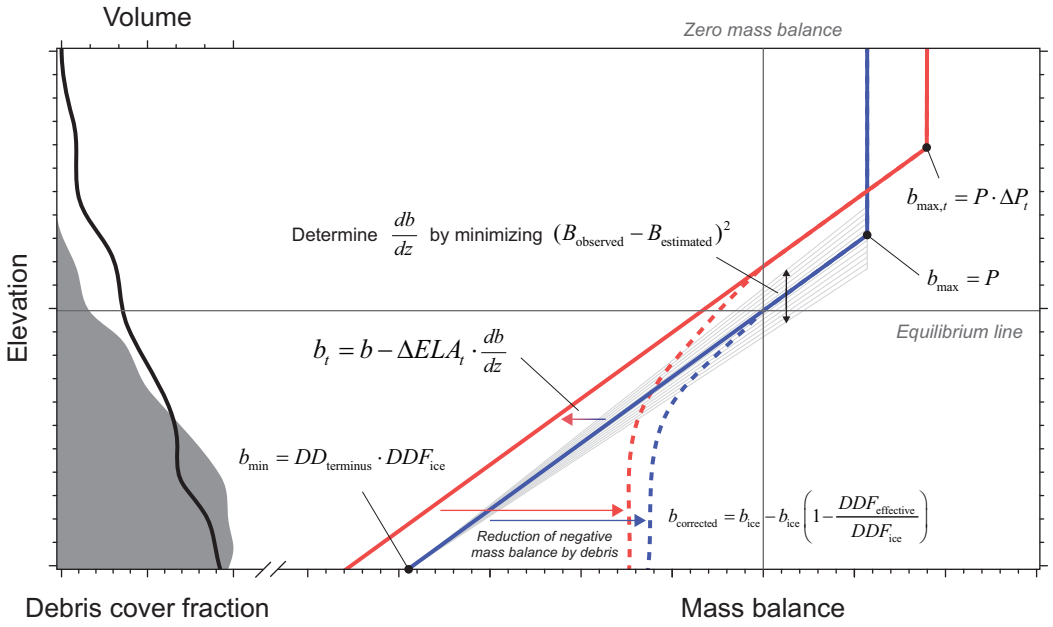

Figure S4 | Concept of the mass balance gradient model. The schematic figure shows the MBG approach used in this study with idealized mass balance curves for the current (blue) and future (red), debris-cover fraction (grey), and debris-corrected mass balances (dashed lines).

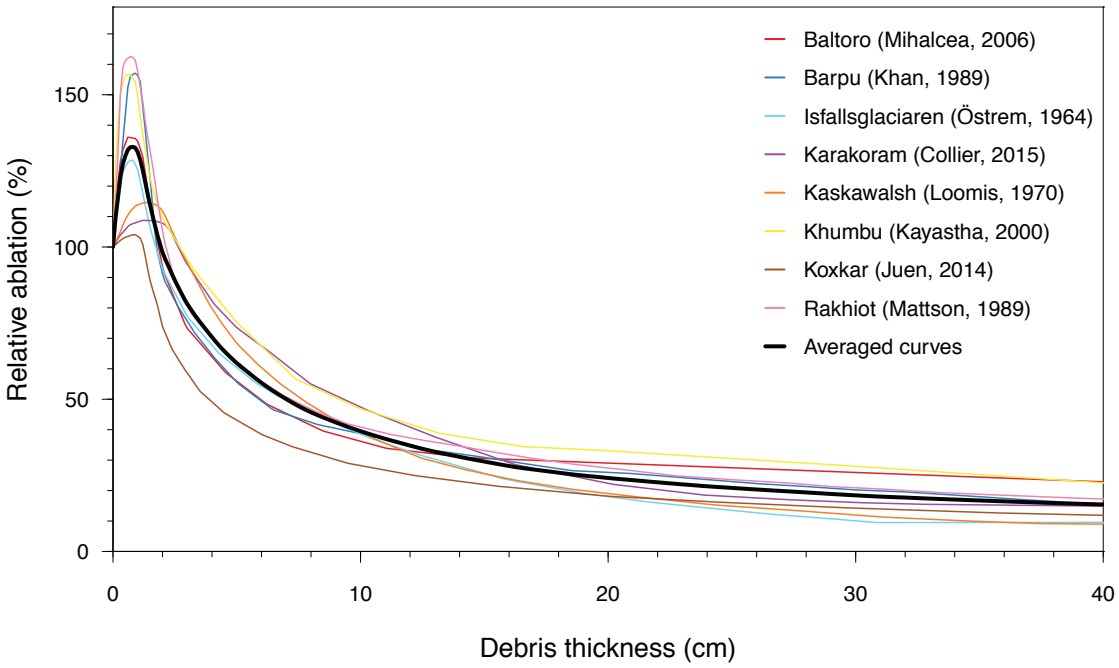

Figure S5 | Ice ablation versus debris thickness. The figure shows ablation under debris cover relative to debris-free ice ablation determined for different glaciers[14,43–47]. The average of the curves is used in the mass balance gradient model to calculate reduction of ice ablation by debris.

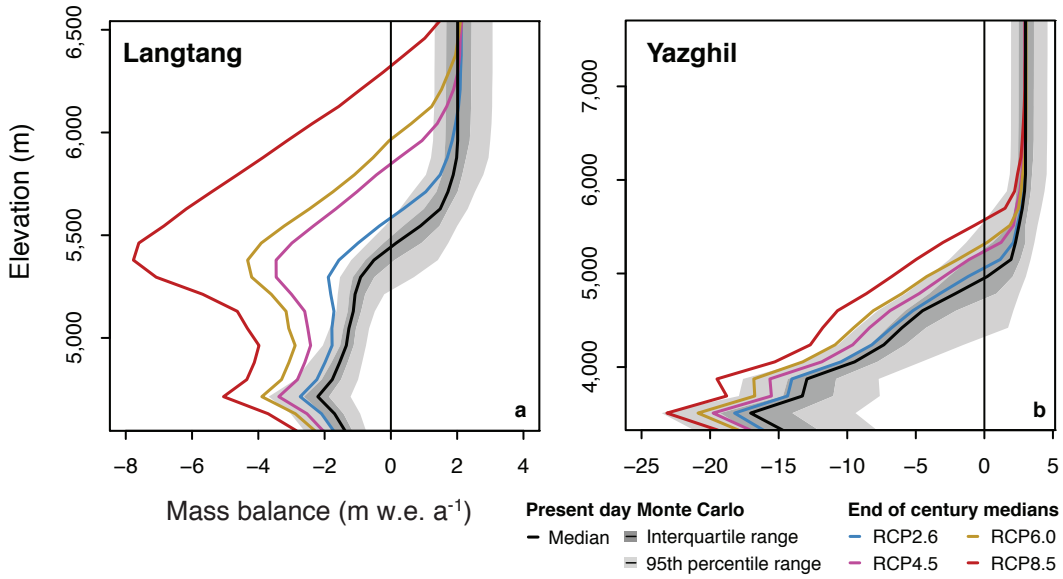

Figure S6 | Examples of mass balance curves fitted using the MBG model. The panels show the median and the spread of mass balance curves for the present day that follow from the Monte Carlo parameter ensemble for both Langtang (**a**) and Yazghil (**b**). Additionally, median mass balance curves are plotted for each RCP ensemble in the end of century (2071-2100).

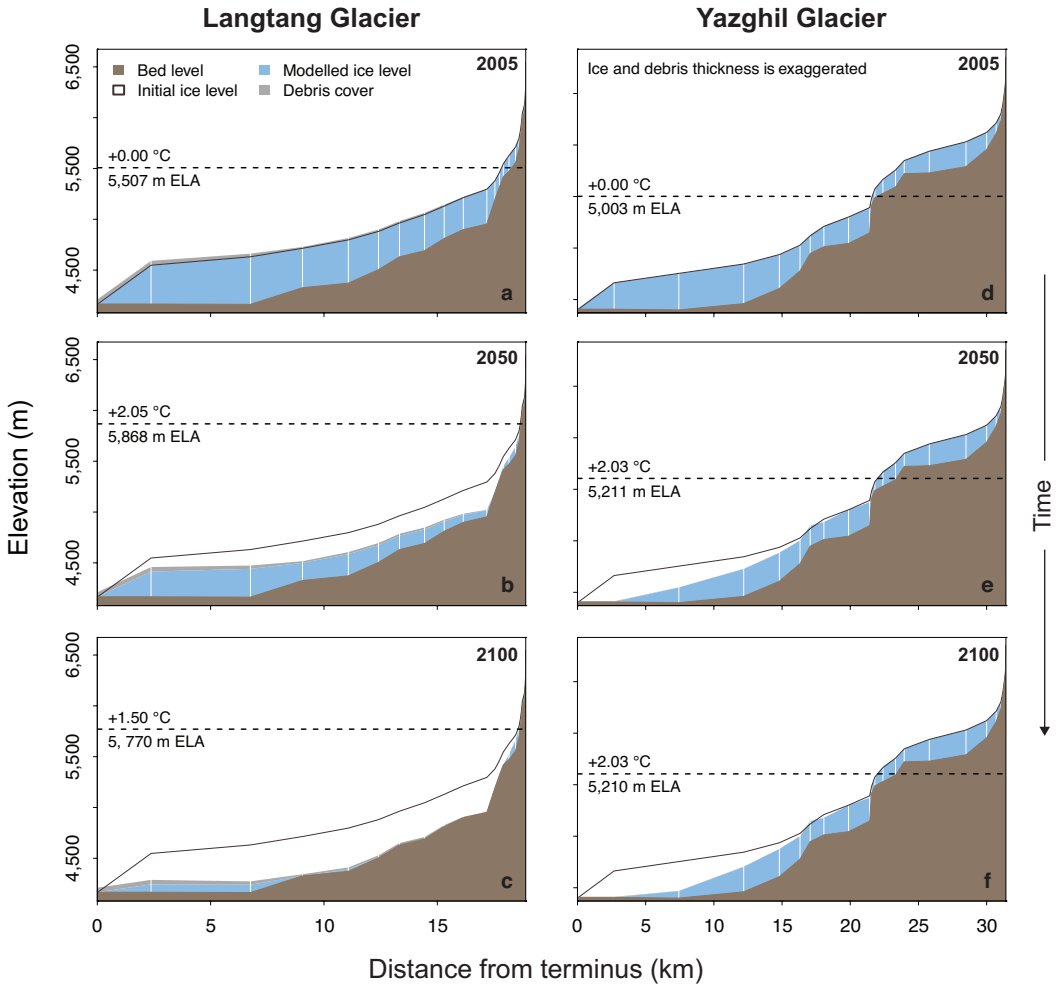

Figure S7 | Schematic cross profiles of modelled ice thicknesses. The panels show examples of modelled reduction in ice thickness at different time steps for Langtang Glacier (**a-c**) and Yazghil Glacier (**d-f**). The separation between the different elevation bands is indicated by the vertical white lines. The forcing used in the figure for both glaciers is MIROC5 RCP2.6 (Table S5).

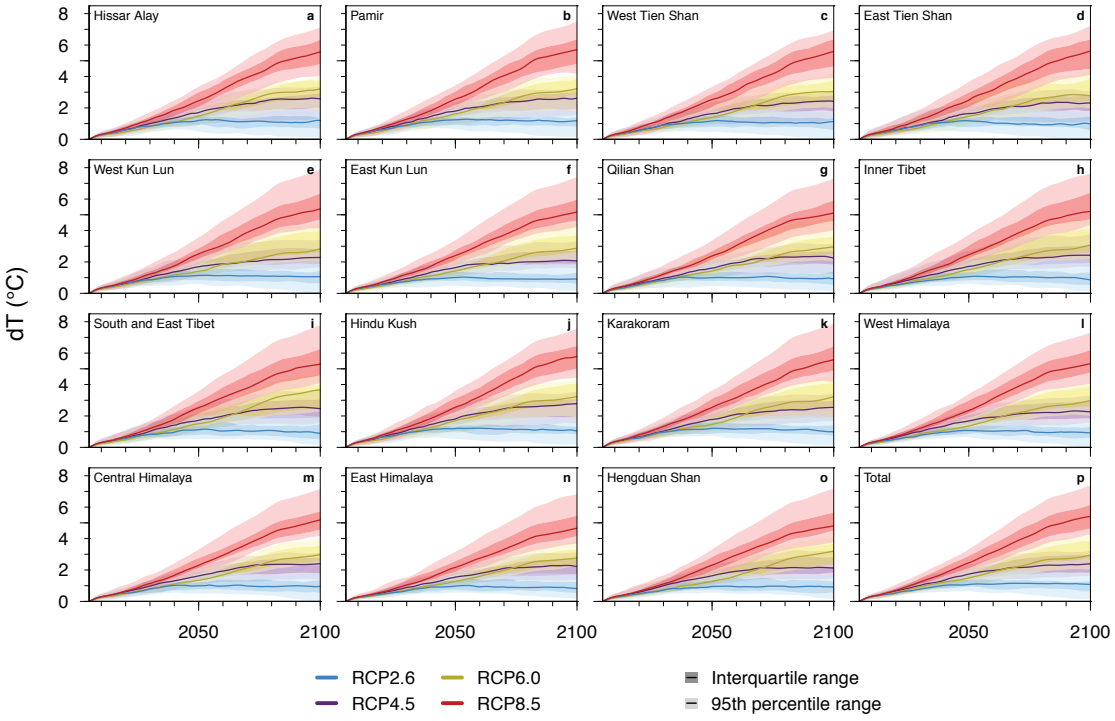

Figure S8 | Temperature forcing over the period 2005-2100. The panels show the transient temperatures that were used to force the mass balance gradient model for the entire model period for all RCPs. Each panel shows a line with the mean temperature and a shading with the RCP ensemble spread for a specific RGI sub-region (**a-o**) or the total HMA (**p**).

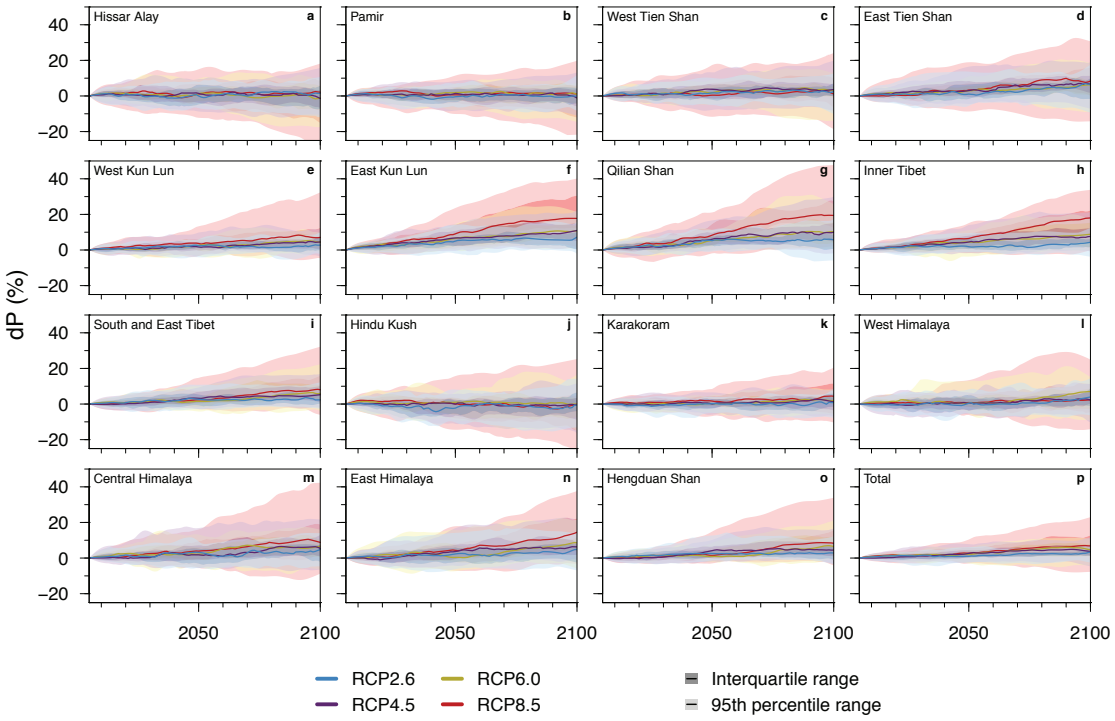

Figure S9 | Precipitation forcing over the period 2005-2100. The panels show the transient precipitation changes that were used to force the mass balance gradient model for the entire model period for all RCPs. Each panel shows a line with the mean precipitation changes and a shading with the RCP ensemble spread for a specific RGI sub-region (**a-o**) or the total HMA (**p**).

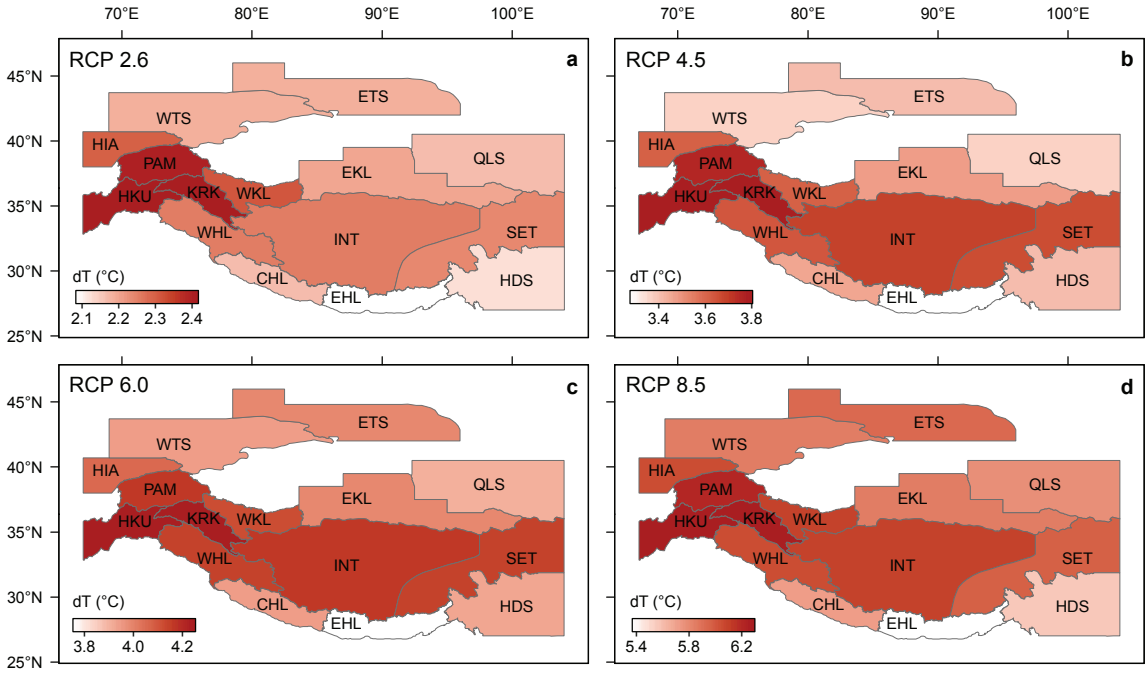

Figure S10 | Mean temperature increases for all four RCPs. Maps with the mean temperature increase at the glaciers of an RGI sub-region between pre-industrial (1851-1880) and end of century (2071-2100) for RCP2.6 (**a**), RCP4.5 (**b**), RCP6.0 (**c**) and RCP8.5 (**d**).

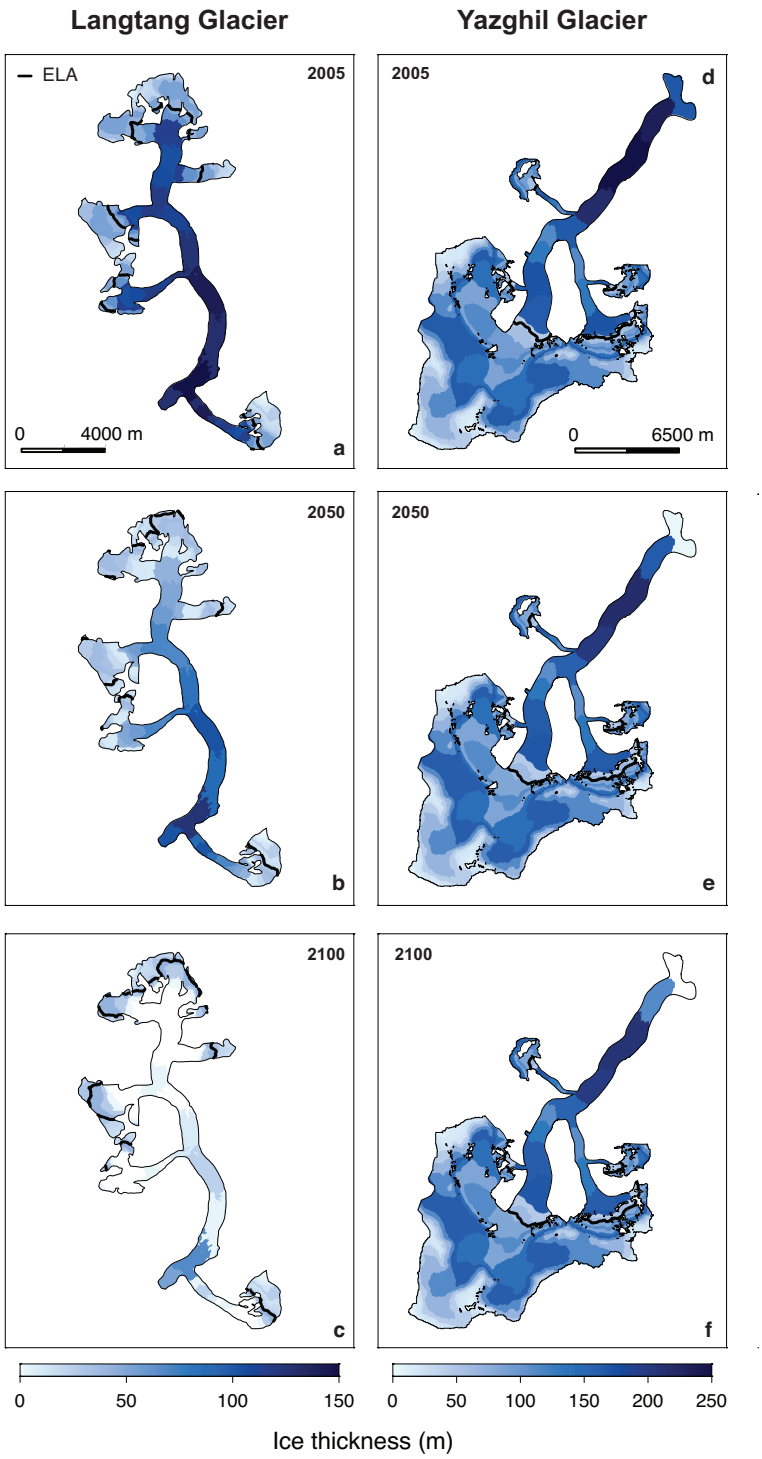

Figure S11 | Example maps of future ice thickness for elevation bands of a glacier. The maps show for Langtang Glacier (**a-c**) and Yazghil Glacier (**d-f**) examples of modelled reduction in average ice thickness per elevation band for three different time steps, which are annotated in each panel. The forcing used in the figure for both glaciers is MIROC5 RCP2.6 (Table S5).

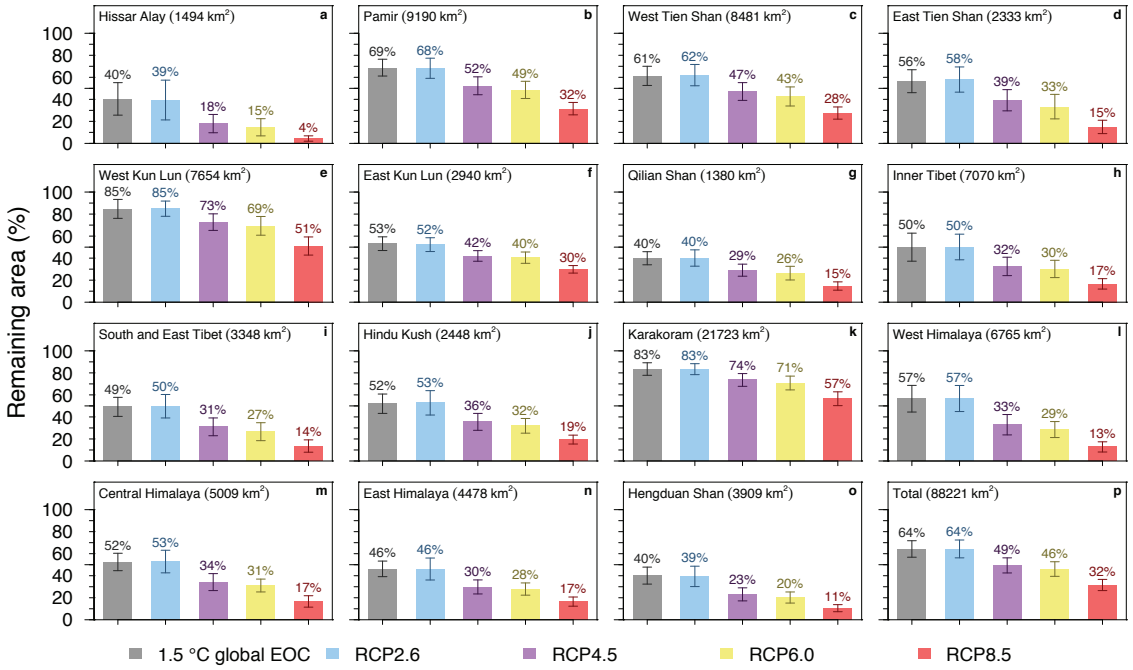

Figure S12 | Remaining glacier area by the end of century. For every RGI sub-region (**a**-**o**) bar plots show the glacierised area that will remain in the end of century (EOC, 2071-2100) for all RCP ensembles and the models selected for the 1.5 °C scenario (Table S5). The error bars indicate the standard deviation of the ensembles. Remaining areas for the entire HMA are shown in panel **p**.

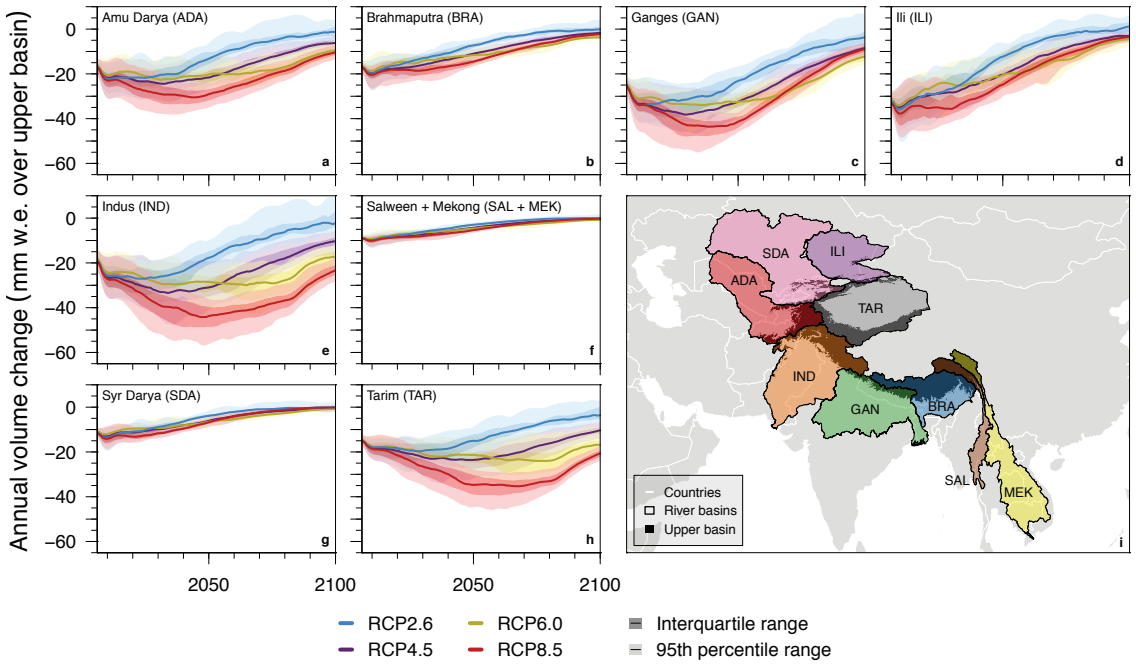

Figure S13 | Annual glacier mass change for major river basins in HMA. The figure shows the transient annual glacier mass changes for the four RCP ensembles, aggregated over the major river basins in HMA that have substantial glacierized areas (**a**-**h**). The mass is expressed in mm w.e. over the upper basin area, i.e. the part of the basin with an elevation higher than its lowest glacier terminus, for better comparison with precipitation. A map of the basins and the upper basin area is shown in panel **i**.

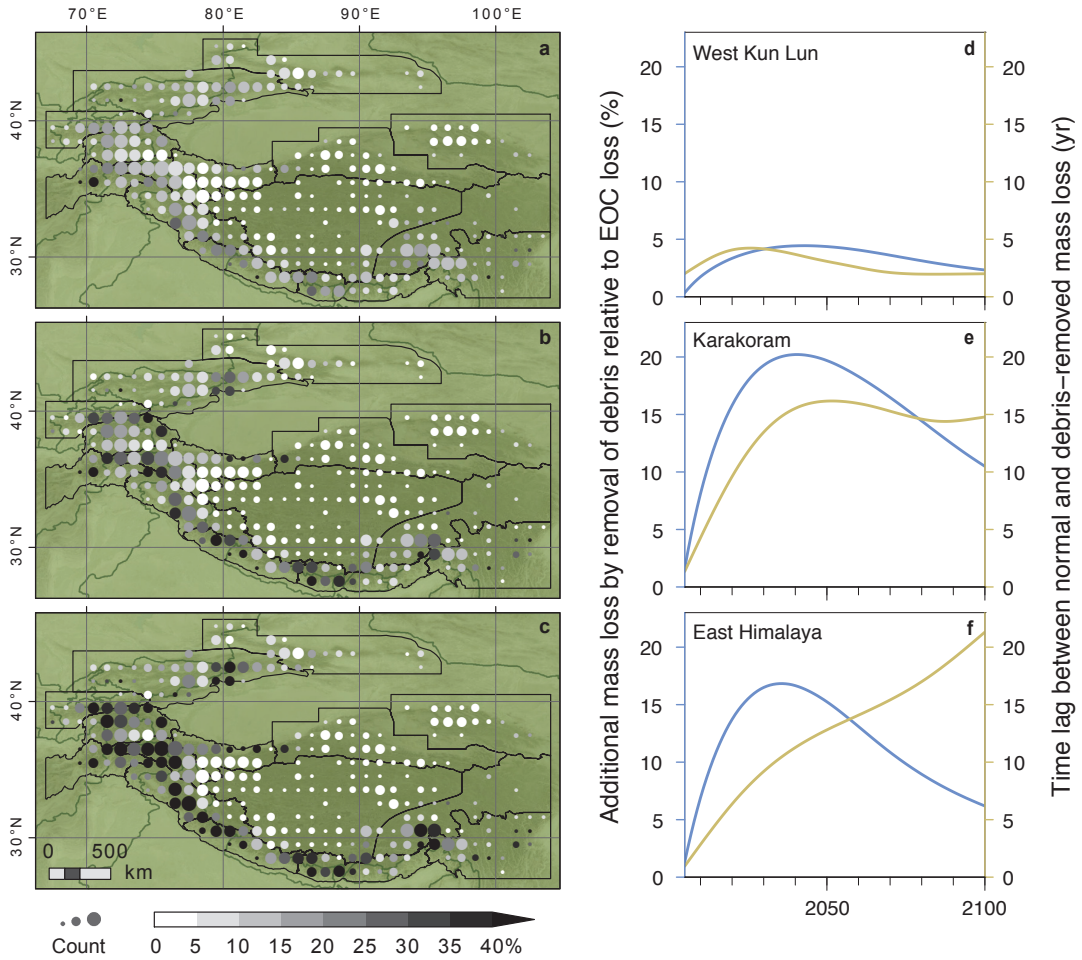

Figure S14 | Spatial patterns in the occurrence of debris-covered glaciers and the impact of debris on delaying climate change impact. Panel **a** shows the relative glacier area that is debris covered, panel **b** shows the relative ice mass stored under debris, and panel **c** shows the relative ice mass stored under debris in the ablation zone (below the equilibrium line altitude). The points represent data aggregated over a 1 by 1 degree grid and the size of points indicate glacier abundance in a grid cell. The panels **d-f** show for three different sub-regions the increase in mass loss that results from a model experiment for which all debris cover was removed (blue line) and the lead in glacier response this yields (orange line).

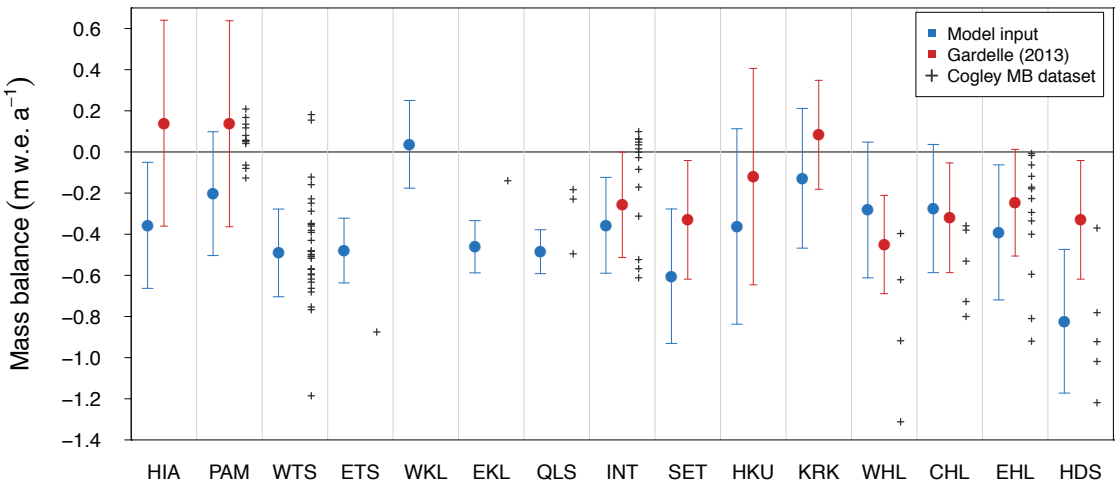

Figure S15 | Comparison of mass balance data. A comparison of the regional mass balance means and inter-glacier standard deviations that were used to force the model (blue) with those determined from data of a large-scale geodetic study[50] (red). Mass balances of the Cogley GMBAL dataset[53] (release 1501) available for glaciers in the RGI sub-regions that fall in the period 2000-2010 (*n=91*) are plotted as grey crosses.

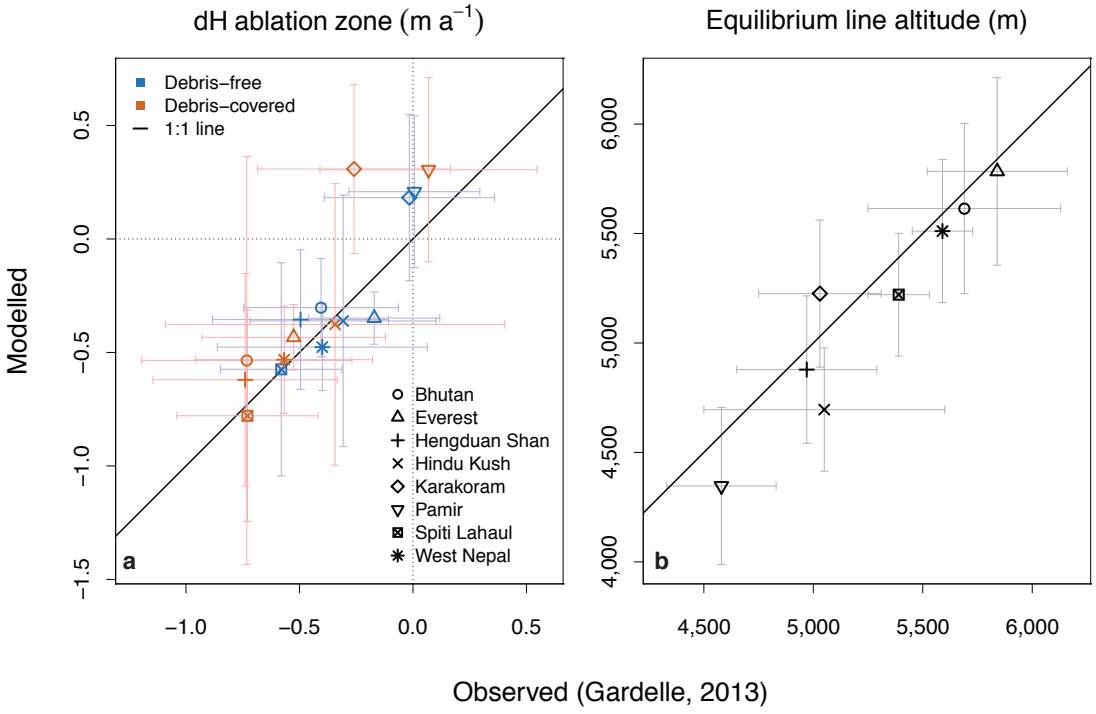

Figure S16 | Validation of modelled elevation change and ELA. Modelled versus observed[50] elevation changes of the ablation zone, shown separately for debris-free and debris-covered tongues (**a**). Modelled ELAs versus reported ELAs[50] for the same regions (**b**). The points denote the regional mean and the whiskers the standard deviation.

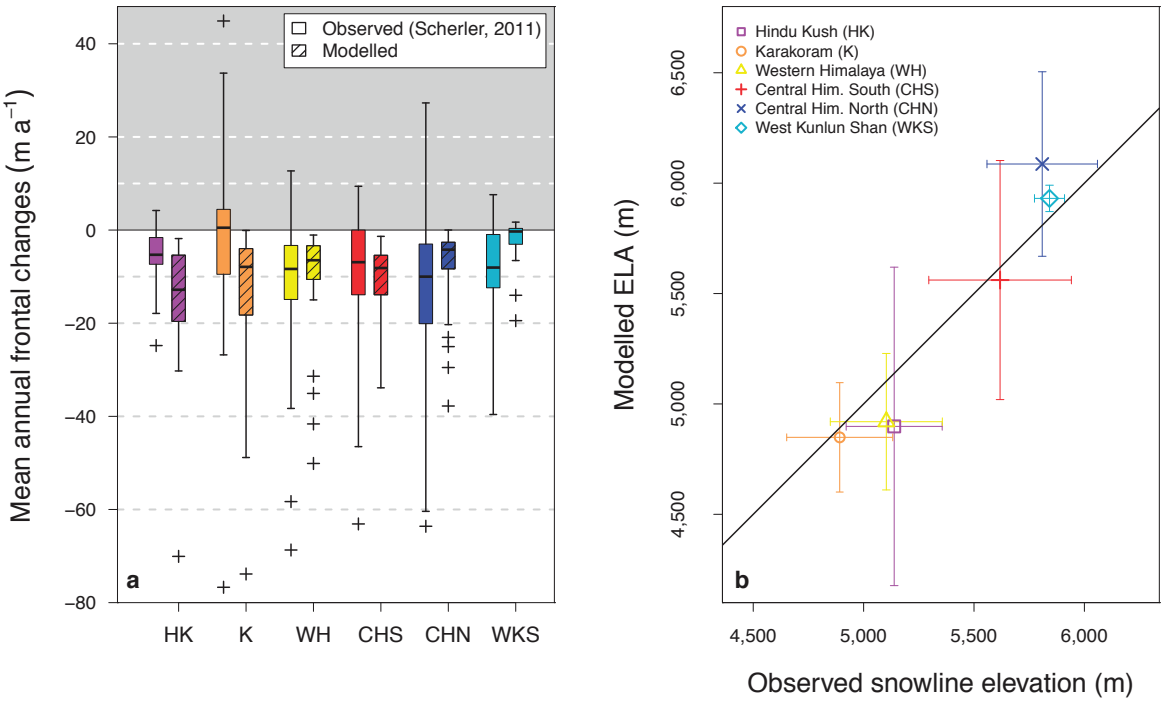

Figure S17 | Validation of frontal changes and ELA. Modelled versus observed[55] fontal changes of glacier tongues (**a**). The horizontal bars denote the median, the boxes the interquartile range, and the crosses denote outliers that are outside 2.5 times the interquartile range. Panel **b** shows modelled ELAs versus estimated snow line elevations[55] for the same regions. The points denote the regional mean and the whiskers the standard deviation.

Table S1 | Glacier statistics for every RGI sub-region. Processed glaciers are those on which the analysis was performed, i.e. glaciers larger 0.4 km^2. Processed area was determined from RGI metadata. Processed volume was determined using the GlabTop2 model results, which was limited to glaciers that are larger than 25 Landsat pixels (n=83,754).

Region	Glaciers	Processed glaciers	Processed glaciers (%)	Processed area (%)	Processed volume (%)
Hissar Alay	3,151	942	29.9	80.9	98.5
Pamir	10,234	3,737	36.5	88.0	99.5
West Tien Shan	9,739	3,388	34.8	89.0	99.4
East Tien Shan	5,227	1,461	28.0	81.7	98.4
West Kun Lun	5,396	2,281	42.3	94.1	99.8
East Kun Lun	3,519	1,275	36.2	90.5	99.7
Qilian Shan	2,730	850	31.1	84.3	98.4
Inner Tibet	9,365	3,093	33.0	89.2	99.4
South Tibet	5,066	1,582	31.2	86.2	99.1
Hindu Kush	4,401	1,298	29.5	83.3	99.0
Karakoram	13,759	4,963	36.1	94.9	99.9
West Himalaya	9,832	3,194	32.5	87.0	99.3
Central Himalaya	4,529	2,015	44.5	92.0	99.5
East Himalaya	4,237	1,750	41.3	91.4	99.6
Hengduan Shan	4,352	1,758	40.4	89.3	99.4
Total	95,537	33,587	35.2	90.2	99.3

Table S2 | Error matrix and statistics that show the accuracy of the debris classification. The error matrix is based on a stratified sample of 1,000 random points for which ground truth was determined visually. For 15 of the random samples ground truth could not be determined accurately. Classification accuracy statistics[33] calculated from the error matrix are shown in the table as well as class abundances for the entire composite mosaic.

Error matrix	*Ground truth*		
Classification	Debris-free	Debris-covered	Lake
Debris-free	371	19	0
Debris-covered	21	373	4
Lake	21	22	154
28% of debris samples on slope >24°			
Error statistics			
Producer's accuracy	90%	90%	97%
User's accuracy	95%	94%	78%
Overall accuracy	91%		
Kappa value	0.86		
Class abundance	102,202,797 (85.9%)	16,501,140 (13.9%)	237,475 (0.2%)

Table S3 | Observed regional mass balances. The table shows the regional mass balances and mass balance standard deviations that were used to run the MBG model. The values were taken from various remote sensing and in situ studies[5,21,22,48,49,51,52].

Region	Observed MB (m)	MB source	Area-weighted SD (m)	SD source
Hissar Alay	-0.36	Kääb 2015	0.31	-
Pamir	-0.20	Kääb 2015	0.30	Zhang 2016
West Tien Shan	-0.49	Farinotti 2015	0.21	Sorg 2015
East Tien Shan	-0.48	Farinotti 2015	0.16	Sorg 2015
West Kun Lun	0.04	Kääb 2015	0.21	Ke 2015
East Kun Lun	-0.46	Kääb 2015	0.13	Ke 2015
Qilian Shan	-0.49	Kääb 2015	0.11	-
Inner Tibet	-0.36	Kääb 2015	0.23	Yao 2012
South Tibet	-0.60	Kääb 2015	0.33	Yao 2012
Hindu Kush	-0.36	Kääb 2015, Gardner 2013	0.48	Gardelle 2013
Karakoram	-0.13	Kääb 2015	0.34	Gardelle 2013
West Himalaya	-0.28	Kääb 2015	0.33	Gardelle 2013
Central Himalaya	-0.28	Kääb 2015	0.31	Gardelle 2013
East Himalaya	-0.40	Kääb 2015	0.33	Gardelle 2013
Hengduan Shan	-0.82	Kääb 2015, Gardner 2013	0.35	Gardelle 2013, Yao 2012

Table S4 | Model parameters that were used in the Monte Carlo sampling. The table shows the parameters for which Monte Carlo sampling was used. For each parameter, the type of statistical distribution, the mean, the standard deviation, and the range is given. The values and ranges for the degree-day factor[36] and debris thickness[26,41–43] were estimated from literature.

Parameter	Distribution	μ	σ	min	max
Degree-day sum ($°C^{-1}\ d^{-1}$)	Gaussian	WFDEI climatology	$\sigma/\sqrt{n_{years}}$	-	-
DDF debris-free ice (mm w.e. $°C^{-1}\ d^{-1}$)	Truncated Gaussian	7	2	0	Inf
Debris thickness (cm)	Truncated Gaussian	50	20	0	Inf
Precipitation changes (-)	Truncated Gaussian	1	0.33	0.5	2
Observed mass balance (m)	Gaussian	Table S3	Table S3	-	-

Table S5 | CMIP5 climate models used for climate forcing. The table shows the models part of each RCP ensemble of CMIP5 GCMs that are used to force the mass balance gradient model. For each model the global and HMA dT (˚C) and dP (%) are shown for both pre-industrial to end of century and present to end of century. Models part of the 1.5 ˚C EOC ensemble are flagged with an asterisk.

RCP	Model run	Global dT 1851-1880 – 2071-2100	Regional dT 1851-1880 – 2071-2100	Regional dP 1851-1880 – 2071-2100	Regional dT 1996-2015 – 2071-2100	Regional dP 1996-2015 – 2071-2100
RCP2.6	bcc-csm1-1-m_r1i1p1	1.86	2.36	6.4	0.83	2.9
RCP2.6	bcc-csm1-1_r1i1p1	1.77	2.20	3.5	0.80	2.8
RCP2.6	BNU-ESM_r1i1p1	2.15	2.65	7.2	1.16	3.4
RCP2.6	CanESM2_r1i1p1	2.24	2.91	19.4	1.39	8.3
RCP2.6	CCSM4_r1i1p1	1.82	2.09	5.1	0.53	2.0
RCP2.6	CESM1-CAM5_r1i1p1	1.97	2.01	16.0	1.29	1.4
RCP2.6	CNRM-CM5_r1i1p1	1.70	1.92	11.7	1.12	2.4
RCP2.6	CSIRO-Mk3-6-0_r1i1p1	1.88	2.45	10.6	1.44	4.2
RCP2.6	EC-EARTH_r8i1p1	1.85	2.45	9.6	0.72	1.3
RCP2.6	FGOALS_g2_r1i1p1	1.13	1.98	2.3	0.84	-1.9
RCP2.6	FIO-ESM_r1i1p1	0.89	1.06	-6.3	-0.58	-7.2
RCP2.6	GISS-E2-H_r1i1p1	1.62	2.36	5.8	0.90	2.3
RCP2.6	GISS-E2-R_r1i1p1	1.05	1.52	9.3	0.27	1.5
RCP2.6	HadGEM2-AO_r1i1p1*	1.57	1.75	5.9	1.15	5.2
RCP2.6	HadGEM2-ES_r2i1p1	1.80	1.87	0.5	1.29	3.3
RCP2.6	IPSL-CM5A-LR_r1i1p1	2.23	3.46	-1.6	1.34	3.6
RCP2.6	IPSL-CM5A-MR_r1i1p1	1.94	3.23	-5.4	1.24	-3.2
RCP2.6	MIROC-ESM-CHEM_r1i1p1	2.35	3.05	3.5	1.82	1.5
RCP2.6	MIROC-ESM_r1i1p1	2.33	3.21	4.9	2.00	2.8
RCP2.6	MIROC5_r1i1p1*	1.49	2.58	14.2	1.84	6.0
RCP2.6	MPI-ESM-LR_r1i1p1*	1.58	2.16	0.7	0.41	2.7
RCP2.6	MPI-ESM-MR_r1i1p1*	1.59	2.14	3.4	0.42	1.0
RCP2.6	MRI-CGCM3_r1i1p1	1.34	1.57	13.3	0.86	3.1
RCP2.6	NorESM1-M_r1i1p1*	1.40	2.24	3.4	1.10	0.6
RCP2.6	NorESM1-ME_r1i1p1*	1.43	2.15	5.1	1.32	-1.9
RCP4.5	ACCESS1-0_r1i1p1	2.63	4.01	4.4	2.92	3.4
RCP4.5	ACCESS1-3_r1i1p1	2.44	2.96	4.8	2.61	2.8
RCP4.5	bcc-csm1-1-m_r1i1p1	2.50	3.31	9.1	1.67	8.0
RCP4.5	bcc-csm1-1_r1i1p1	2.48	3.27	6.5	1.83	2.6
RCP4.5	BNU-ESM_r1i1p1	3.16	3.90	3.3	2.50	-3.9
RCP4.5	CanESM2_r1i1p1	3.04	4.46	18.2	2.99	10.8
RCP4.5	CCSM4_r1i1p1	2.56	3.29	7.3	1.72	4.0
RCP4.5	CESM1-BGC_r1i1p1	2.45	3.43	6.5	1.86	3.8
RCP4.5	CESM1-CAM5_r1i1p1	2.76	3.41	18.7	2.62	9.4
RCP4.5	CMCC-CM_r1i1p1	2.73	3.72	9.4	2.71	6.3
RCP4.5	CMCC-CMS_r1i1p1	2.70	3.97	1.6	2.73	-0.4
RCP4.5	CNRM-CM5_r1i1p1	2.51	2.91	14.8	2.23	4.9
RCP4.5	CSIRO-Mk3-6-0_r1i1p1	2.66	3.74	9.9	2.63	7.4
RCP4.5	EC-EARTH_r8i1p1	2.58	3.33	13.6	1.71	11.3
RCP4.5	FGOALS_g2_r1i1p1	1.82	3.02	2.9	1.68	0.4
RCP4.5	FIO-ESM_r1i1p1	1.85	2.54	-5.2	0.89	-3.8
RCP4.5	GISS-E2-H-CC_r1i1p1	2.34	3.94	10.1	1.87	6.5
RCP4.5	GISS-E2-H_r1i1p1	2.38	3.60	12.0	2.17	7.7
RCP4.5	GISS-E2-R-CC_r1i1p1	1.85	3.11	12.7	1.54	6.4
RCP4.5	GISS-E2-R_r1i1p1	1.76	2.89	1.1	1.58	0.6
RCP4.5	HadGEM2-AO_r1i1p1	2.87	3.86	3.7	3.02	4.6
RCP4.5	HadGEM2-CC_r1i1p1	2.44	2.87	2.1	2.86	7.7
RCP4.5	HadGEM2-ES_r2i1p1	2.95	3.55	3.4	2.98	6.0
RCP4.5	inmcm4_r1i1p1	1.81	2.95	-0.1	1.51	1.3
RCP4.5	IPSL-CM5A-LR_r1i1p1	3.10	5.08	-5.2	2.93	0.3
RCP4.5	IPSL-CM5A-MR_r1i1p1	3.05	5.25	-4.6	3.12	2.4
RCP4.5	IPSL-CM5B-LR_r1i1p1	2.47	2.90	8.8	1.80	5.0
RCP4.5	MIROC-ESM-CHEM_r1i1p1	3.17	4.37	9.3	3.36	6.9

RCP4.5	MIROC-ESM_r1i1p1	3.15	4.50	6.7	3.24	5.2
RCP4.5	MIROC5_r1i1p1	2.12	4.08	15.5	3.17	4.5
RCP4.5	MPI-ESM-LR_r1i1p1	2.39	3.86	-4.4	2.17	-2.3
RCP4.5	MPI-ESM-MR_r1i1p1	2.45	3.74	3.9	2.02	4.1
RCP4.5	MRI-CGCM3_r1i1p1	1.99	2.64	19.8	1.90	8.9
RCP4.5	NorESM1-M_r1i1p1	2.12	3.33	3.1	2.33	1.4
RCP4.5	NorESM1-ME_r1i1p1	2.16	3.42	5.6	2.52	-1.6
RCP6.0	bcc-csm1-1-m_r1i1p1	2.90	4.09	4.8	2.52	1.3
RCP6.0	bcc-csm1-1_r1i1p1	2.83	3.84	3.8	2.25	0.0
RCP6.0	CCSM4_r1i1p1	2.94	3.70	6.9	2.05	2.2
RCP6.0	CESM1-CAM5_r1i1p1	3.15	4.05	20.8	3.31	9.9
RCP6.0	CSIRO-Mk3-6-0_r1i1p1	2.74	3.57	16.1	2.52	13.6
RCP6.0	FIO-ESM_r1i1p1	2.32	3.07	-5.0	1.33	-4.6
RCP6.0	GISS-E2-H_r1i1p1	2.64	3.94	12.4	2.59	7.5
RCP6.0	GISS-E2-R_r1i1p1	2.64	3.94	1.3	2.59	0.8
RCP6.0	HadGEM2-AO_r1i1p1	2.85	3.69	7.1	3.02	5.7
RCP6.0	HadGEM2-ES_r2i1p1	3.31	3.91	1.4	3.50	6.2
RCP6.0	IPSL-CM5A-LR_r1i1p1	3.39	5.61	-9.3	3.41	-5.6
RCP6.0	IPSL-CM5A-MR_r1i1p1	3.34	5.65	-6.4	3.67	-3.0
RCP6.0	MIROC-ESM-CHEM_r1i1p1	3.57	5.26	7.5	3.98	5.9
RCP6.0	MIROC-ESM_r1i1p1	3.49	5.18	8.8	3.90	7.9
RCP6.0	MIROC5_r1i1p1	2.35	4.40	20.0	3.70	9.0
RCP6.0	MRI-CGCM3_r1i1p1	2.18	2.93	23.9	2.26	10.7
RCP6.0	NorESM1-M_r1i1p1	2.32	3.66	8.2	2.66	5.3
RCP6.0	NorESM1-ME_r1i1p1	2.38	3.56	9.6	2.72	3.7
RCP8.5	ACCESS1-0_r1i1p1	4.26	6.34	4.9	5.25	5.1
RCP8.5	ACCESS1-3_r1i1p1	4.17	4.88	8.6	4.44	5.7
RCP8.5	bcc-csm1-1_r1i1p1	4.12	5.64	8.8	4.14	7.2
RCP8.5	BNU-ESM_r1i1p1	5.10	6.54	-2.9	5.08	-6.9
RCP8.5	CanESM2_r1i1p1	4.99	7.41	33.1	5.94	22.2
RCP8.5	CCSM4_r1i1p1	4.34	5.76	9.0	4.20	7.2
RCP8.5	CESM1-BGC_r1i1p1	4.20	5.71	8.6	4.09	6.0
RCP8.5	CESM1-CAM5_r1i1p1	4.37	5.96	26.0	5.05	14.7
RCP8.5	CMCC-CM_r1i1p1	4.50	6.63	11.7	5.75	7.9
RCP8.5	CMCC-CMS_r1i1p1	4.56	6.76	2.9	5.50	2.0
RCP8.5	CNRM-CM5_r1i1p1	3.92	4.90	24.4	4.12	15.6
RCP8.5	CSIRO-Mk3-6-0_r1i1p1	4.21	5.80	21.4	4.81	13.2
RCP8.5	EC-EARTH_r8i1p1	4.11	5.65	22.2	4.05	17.9
RCP8.5	FGOALS_g2_r1i1p1	3.30	5.03	11.5	3.73	8.0
RCP8.5	FIO-ESM_r1i1p1	4.00	5.33	-11.5	3.75	-9.9
RCP8.5	GISS-E2-H_r1i1p1	3.66	5.73	15.3	4.23	12.9
RCP8.5	GISS-E2-R_r1i1p1	2.95	4.73	1.8	3.55	1.3
RCP8.5	HadGEM2-AO_r1i1p1	4.34	5.79	7.9	5.13	6.7
RCP8.5	HadGEM2-CC_r1i1p1	4.55	5.78	1.2	5.71	5.1
RCP8.5	HadGEM2-ES_r2i1p1	4.79	6.00	2.3	5.41	5.3
RCP8.5	inmcm4_r1i1p1	3.08	5.22	2.3	3.87	1.6
RCP8.5	IPSL-CM5A-LR_r1i1p1	5.18	8.33	-10.8	6.14	-6.0
RCP8.5	IPSL-CM5A-MR_r1i1p1	5.01	8.57	-7.4	6.48	-4.1
RCP8.5	IPSL-CM5B-LR_r1i1p1	4.02	5.20	16.4	4.13	11.3
RCP8.5	MIROC-ESM-CHEM_r1i1p1	5.27	8.10	10.2	6.89	7.2
RCP8.5	MIROC-ESM_r1i1p1	5.06	7.87	8.0	6.60	5.9
RCP8.5	MIROC5_r1i1p1	3.59	6.20	32.7	5.44	20.7
RCP8.5	MPI-ESM-LR_r1i1p1	4.15	6.58	-3.3	5.02	-2.9
RCP8.5	MPI-ESM-MR_r1i1p1	4.11	6.04	5.5	4.37	4.6
RCP8.5	MRI-CGCM3_r1i1p1	3.41	5.03	31.2	4.31	17.9
RCP8.5	NorESM1-M_r1i1p1	3.53	5.51	6.0	4.44	3.1
RCP8.5	NorESM1-ME_r1i1p1	3.68	5.62	7.8	4.73	1.9